

MEASUREMENT OF PRIOR AUSTENITE GRAIN SIZE IN BAINITE/MARTENSITE MICROSTRUCTURES

L. Morales-Rivas¹, V.A. Yardley², C. Capdevila¹, C. Garcia-Mateo¹, H. Roelofs³, F.G. Caballero¹

¹*National Center for Metallurgical Research (CENIM-CSIC), Avda Gregorio del Amo, 8; Madrid, E-28040, Spain.*

²*Institute for Materials, Ruhr-Universität Bochum, 44780 Bochum, Germany.*

³*R&D, Swiss Steel AG, Emmenweidstr. 90, CH-6020 Emmenbrücke, Switzerland.*

Corresponding author:

C. Carlos Garcia-Mateo.

e-mail address: cgm@cenim.csic.es

Telephone: +34 91 553 89 00

Abstract:

An alternative procedure for indirect and automatic measurement of the prior austenite grain size (PAGS) in bainite/martensite is proposed in this work. It consists in the determination of an effective grain size (EGS) by means of statistical post-processing of electron backscatter diffraction (EBSD) data. The algorithm developed for that purpose, which is available on-line, has been applied to simulated EBSD maps as well as to both a nanocrystalline bainitic steel and a commercial hot-rolled air-cooled steel with a granular bainitic microstructure. The new proposed method has been proven to be robust and results are in good agreement with conventional PAGS measurements. The added value of the procedure comes from its simplicity, as no parent reconstruction is involved during the process, and its suitability for low-magnification EBSD maps, thus allowing a large step-size and coverage of a substantially broader area of the sample than the previous methods reported.

Keywords: EBSD, Prior Austenite Grain Size, Orientation Relationship, Bainite, Martensite.

1 INTRODUCTION

There are many ways to strengthen metallic materials by impeding dislocation movements, such as solid-solution strengthening, precipitation hardening or grain size refinement. The latter is, among all, the most effective and is used for the strengthening of steels. Fine grains prevent a large number of dislocations from piling up against their interfaces, resulting in a low stress concentration and thus impeding the transmission of plasticity, thereby increasing the strength of the material. Unlike the other mechanisms, grain refinement is also beneficial for toughness, since interfaces are barriers against crack propagation.

In steels, an important parameter controlling the refinement of the microstructure is the Prior Austenite Grain Size (PAGS) due to its strong influence on the kinetics of austenite decomposition. A reduction of the PAGS leads to an increase in the grain surface per unit volume. This means that for transformations involving heterogeneous nucleation at the grain boundaries, such as in bainite and martensite, the increase in the number density of nucleation sites leads invariably to an increase in the nucleation rate and hence, a finer product grain size because of impingement [1,2]. For the case of bainite transformation, this effect generally comes accompanied by an increase in the transformation rate, which is critical for the industrialization of recently developed low-temperature bainite [2,3,4].

There have been many approaches to the determination of the PAGS. Among metallographic methods intended to reveal the Prior Austenite Grain Boundary (PAGB) at room temperature, chemical etching alone is the simplest one. However, no single etchant is capable of revealing the PAGB in all types of steels, since it depends on the microstructure and chemical composition; in practice, considerable trial and error is involved in many attempts to bring out the grain boundaries sufficiently to permit grain size measurements, and in some cases, all attempts result in failure. Other methods involve a complex heat treatment, such as interrupted cooling or the gradient-quenching, and even in some cases a previous and special sample surface preparation, like thermal etching, which make these methods only suitable to reveal PAGB on samples reproduced at the laboratory, not in industrial samples [5,6], which in many cases are subjected to thermomechanical treatments. The same

problem arises when *in-situ* observation of the austenitic grains is made by means of high temperature microscopy, using modified optical, electron or confocal scanning violet laser microscopes, capable of operating at temperatures within the austenitic range [5,7,8,9].

The development of the Electron Backscatter Diffraction (EBSD) technology coupled to the Scanning Electron Microscope (SEM) has brought new possibilities in the application of the electron backscatter diffraction technique to the investigation of phase transformations in steels, as has recently been reviewed by Gourgues-Lorenzon [10]. The wide variety of results obtained using this technique is illustrated and discussed in that work, focusing on thermodynamics and kinetics of phase transformations, solidification, solid state phase transformations, environmentally assisted reactions and thin film deposition. It is concluded that the measured grain size and grain connectivity strongly depend on the definition of grains given by the EBSD user, which emphasise the importance of the present contribution in terms of defining properly the prior austenite grain size.

For every class of polycrystalline materials, the scientific study of grain boundaries as well as the increasingly widespread practice of grain boundary engineering, rely, heavily, on visual representation for the analysis of boundary statistics and their connectivity. Traditional methods of grain boundary representation drastically simplify misorientations into discrete categories such as coincidence vs. non-coincidence boundaries, special vs. general boundaries, and low- vs. high-angle boundaries. Such rudimentary methods are used either because there has historically been no suitable mathematical structure with which to represent the relevant grain boundary information, or, where there are existing methods they are extremely unintuitive and cumbersome to use. Patala et al [11] review recent developments that significantly advance our ability to represent a critical part of the grain boundary space: the misorientation information. Two specific topics are reviewed in detail, each of which has recently enjoyed the development of an intuitive and rigorous framework for grain boundary representation: (i) the mathematical and graphical representation of grain boundary misorientation statistics, and (ii) colorized maps or micrographs of grain boundary misorientation. At the outset, conventions for parameterization of misorientations, projections of misorientation

information into lower dimensions, and sectioning schemes for the misorientation space are established. Then, the recently developed hyperspherical harmonic formulation for the description of orientation distributions is extended to represent grain boundary statistics. This allows an intuitive representation of the distribution functions using the axis–angle parameterization that is physically related to the boundary structure. Finally, recently developed coloring schemes for grain boundaries are presented and the color legends for interpreting misorientation information are provided. This allows micrographs or maps of grain boundaries to be presented in a colorized form which, at a glance, reveals all of the misorientation information in an entire grain boundary network, as well as the connectivity among different boundary misorientations. These new and improved methods of representing grain boundary misorientation information are expected to be powerful tools for grain boundary network analysis as the practice of grain boundary engineering becomes a routine component of the materials design paradigm.

An alternative application of EBSD to the field of phase-transformations in steels is the determination of the PAGS from the final microstructure. If there is homogeneously dispersed retained austenite, for example blocks and films in a matrix of bainitic ferrite or martensite, it is possible to infer the parent microstructure before transformation. Software tools such as the MATLAB toolbox MTEX [12] make this task even easier, by means of functions that allow features indexed as austenite and sharing a crystallographic orientation to be joined, filling the space in between and reconstituting the original PAG. However, retained austenite is not always present in bainitic/martensitic microstructures, and if it is, it may be difficult to index it by EBSD. Driven by the growing interest in bainitic/martensitic steels, new methods of parent reconstruction have been developed, making use of the fact that bainite/martensite maintains a fixed Orientation Relationship (OR) with its parent austenite; well-known OR of this type include Kurdjumov-Sachs (K-S) [13], Table 1, which is close to the OR observed experimentally in upper bainite [14] or Nishiyama-Wassermann (N-W) OR [15,16]. As a result of the OR, the bainitic-ferrite/martensite variants from a single PAG exhibit only a limited set of misorientations to one another. A common way to perform the parent reconstruction is the

assessment of pole figures from areas of the orientation map selected manually by the user; checking every time if the pole figure of the currently selected area matches well with the expected pole figure from bainite/martensite variants belonging to one single PAG. However, this methodology is not only a slow process but can introduce ambiguities, since the presence of bainite/martensite variants with a high orientation spread is common. This orientation spread includes two contributions: the orientation gradient in the austenite before transformation and the spread around the OR [17,18]. This phenomenon makes built-in functions of commercial analysis software such as the *grain reconstruction* capability in HKL [19], fail in this matter. Such functions allow certain misorientations to be disregarded when grain boundaries are identified, the set of K-S or N-W inter-variant misorientations in our case, but they are not optimized for a reliable parent reconstruction in microstructures exhibiting significant scatter. Other, more sophisticated algorithms for obtaining a reliable parent reconstruction in bainitic/martensitic microstructures based on EBSD data have been developed with the aim of overcoming the difficulties resulting from the orientation spread and other features of the bainitic/martensitic nature that lead to the frequent occurrence of ambiguous variants [17,20,21,22,23,24]. An alternative possibility is to assess the length of prior austenite grain boundaries relative to boundaries between bainitic/martensitic variants, since these can be identified by both the misorientation angle and the misorientation axis [25], avoiding the parent reconstruction process. However, this procedure is similarly affected by the orientation relationship spread, and for optimum results it should be customized for every bainitic/martensitic microstructure, each having a particular orientation relationship, and, moreover, it is likely to be strongly dependant on the EBSD step-size. Another common post-processing tool of EBSD data, the *misorientation profile* (the misorientation angle along a line defined by the user) has been used so far in similar microstructures for purposes other than the determination of the PAGS, for instance, the analysis of the misorientation angle between martensite and austenite across their interface [26]. One could envisage using a large number of such line profiles to obtain the average separation between misorientations that do not correspond to one of the inter-variant orientations, although the problem of scatter would still persist.

Recently, Brahme et al. [27] developed a new statistical method for the evaluation of the long-range dependence of texture in crystalline materials. Their method, based on EBSD, calculates an average misorientation as a function of distance between data points, giving a measure of clustering of texture that is used to determine accurately an Effective Grain Size (EGS). Similarly, Beausir et al. [28] studied grain misorientation in relation to the nearest neighbor's mutual distance using EBSD measurements. The misorientation correlation function was defined as the probability density for the occurrence of a certain misorientation between pairs of grains separated by a certain distance. Scale-invariant spatial correlation between neighbor grains was manifested by a power law dependence of the preferred misorientation vs. inter-granular distance in various materials after diverse strain paths. It is the purpose of the present work to adapt and implement such a distance-misorientation methodology to allow the determination of the PAGS in bainitic/martensitic microstructures by means of an automatic post-processing of EBSD data. The advantage of the method proposed in this work is the lower computational intensity with respect to reconstruction-based methods, making it useful in cases where only a representative value of the PAGS is necessary and more detailed knowledge of the PAG microstructure is not required.

2- METHOD, MATERIAL AND EXPERIMENTAL PROCEDURE

The method proposed in this work for the statistical calculations of the PAGS has been tested using simulated EBSD maps and experimentally validated using two different bainitic microstructures.

2.1 DESCRIPTION OF THE METHOD

The new method proposed in this work to calculate the apparent PAGS involves two steps: the first one is the automatic computation of the *Distance-Disorientation Function* (DDF), and the second step is the determination of an EGS, as proposed by Brahme et al [27], but using a different mathematical parameter, as will be detailed later. In the first step, every possible pair of EBSD data points is considered, not only nearest-neighbor data points; the algorithm collects both the

misorientation angle and the distance between them to calculate the DDF, i.e., the misorientation distributions of data points spaced at different lengths (distances) from each other. The DDF thus constitutes a continuous spectrum between the correlated misorientation distribution (nearest neighbors only) and the uncorrelated misorientation distribution (each point with each other point in the dataset). It is worth mentioning that the DDF is not cumulative, i.e. the parameter distance is the actual length separating data points, therefore it does not include lengths of a lower value. An example of a DDF is plotted in Fig.1, corresponding to the simulated EBSD map 2 in Table 2; this map consists of 30 hexagons of 91 μm size, with a Kurdjumov-Sachs Orientation Relationship (KS-OR) between austenite and martensite. At low distances, most pairs of data points belong to the same PAG, and thus, the distribution presents peaks at those discrete values of misorientations corresponding to the particular orientation relationship between variants resulting from the KS-OR. However at higher distances, the contribution to the distribution of data points that do not share the same PAG is higher, hence, the distribution of misorientations gets closer and closer to the Mackenzie-Handscomb one, which is the density distribution of the misorientation angles between two crystals of cubic symmetry randomly oriented. This convergence can be more clearly seen in the example in Fig. 2, where the misorientation distributions corresponding to the simulated EBSD map 2 in Table 2 are shown in 2D together with a simulated Mackenzie-Handscomb distribution [29,30].

Thus, it is reasonable to think that the evolution of the misorientation distributions with distance must be related to the PAGS. In this sense, the second step of the method consists in the calculation of an EGS as the critical distance value at which the distribution of misorientations stabilizes, changing no longer. For that purpose, the residual sum of squares (RSS) between the Mackenzie-Handscomb distribution and the misorientation distributions is calculated, and plotted vs. distance. The RSS reaches a lower limit at a certain distance, which is the so-called EGS. The parameter EGS as proposed by Brahme *et al.* [27] used the same concept, but was calculated from the evolution curve of the distribution mean vs. distance. In the present work, the EGS is not obtained that way, but RSS vs.

distance, because very different distributions like those in Fig. 2 have similar mean values, within 38° and 41°, making the Brahme *et al.* methodology to calculate EGS unsuitable in this particular scenario.

2.2 TESTING OF THE METHOD USING SIMULATED EBSD DATA

In simulated EBSD maps, PAG sections have been designed as regular hexagons in which a set of data points “indexed” as ferrite have been placed with uniform spacing. Their crystallographic orientations are such that those data points belonging to the same PAG (for example, 1-2 and 4-5 in Fig. 3) have one of the allowed K-S inter-variant misorientations listed in Table 1. All variants are taken to be equally probable and no morphological restriction is imposed. Data points belonging to a different PAG (for example, 2-3 and 2-4 in Fig. 3) hold a random orientation relationship. In this sense, two groups of maps have been simulated:

-Group 1: Three simulated maps, each having a different hexagon size for the PAG sections, while keeping the same step-size, i.e., same density of data points, and the same number of hexagons, so that the effect of the PAGS can be isolated from other geometrical parameters, see Table 2.

-Group 2: Eight simulated maps, all having the same hexagon size, while changing the number of hexagons and/or step-size, so that the sensitivity of the algorithm to geometrical parameters other than the PAGS can be assessed, see Table 3.

The apparent PAGS of the simulated EBSD maps has been calculated as the Feret diameter, i.e. the diameter of the circle having the same area as the corresponding grain section (hexagon). The EGS values calculated from the simulated EBSD maps will be compared to the known corresponding apparent PAGS.

Table 1. Kurdjumov-Sachs orientation relationship in axis/rotation angle notation

Variant no.	Rotation from variant 1
1	None
2	$[0.58, -0.58, 0.58]/60.0^\circ$ or $[0.00, -0.71, -0.71]/70.5^\circ$
3	$[0.00, -0.71, -0.71]/60.0^\circ$
4	$[0.00, 0.71, 0.71]/10.5^\circ$
5	$[0.00, 0.71, 0.71]/60.0^\circ$
6	$[0.00, -0.71, -0.71]/49.5^\circ$
7	$[-0.58, -0.58, 0.58]/49.5^\circ$
8	$[0.58, -0.58, 0.58]/10.5^\circ$
9	$[-0.19, 0.77, 0.61]/50.5^\circ$
10	$[-0.49, -0.46, 0.74]/50.5^\circ$
11	$[0.35, -0.93, -0.07]/14.9^\circ$
12	$[0.36, -0.71, 0.60]/57.2^\circ$
13	$[0.93, 0.35, 0.07]/14.9^\circ$
14	$[0.74, 0.46, -0.49]/50.5^\circ$
15	$[-0.25, -0.63, -0.74]/57.2^\circ$
16	$[0.66, 0.66, 0.36]/20.6^\circ$
17	$[-0.66, 0.36, -0.66]/51.7^\circ$
18	$[-0.30, -0.63, -0.72]/47.1^\circ$
19	$[-0.61, 0.19, -0.77]/50.5^\circ$
20	$[-0.36, -0.60, -0.71]/57.2^\circ$
21	$[0.96, 0.00, -0.30]/20.6^\circ$
22	$[-0.72, 0.30, -0.63]/47.1^\circ$
23	$[-0.74, -0.25, 0.63]/57.2^\circ$
24	$[0.91, -0.41, 0.00]/21.1^\circ$

Table 2. Inputs for group 1 of simulated EBSD maps.

Simulated map	Hexagon size (Apparent PAGS) [μm]	Number of hexagons	Step-size [μm]
1	18	30	4
2	91	30	4
3	182	30	4

Table 3. Inputs for group 2 of simulated EBSD maps.

Simulated map	Hexagon size (Apparent PAGS) [μm]	Number of hexagons	Step-size [μm]
3	182	30	4
4	182	30	8
5	182	9	8
6	182	2	8
7	182	9	4
8	182	9	16
9	182	9	22
10	182	42	8

2.3 EXPERIMENTAL VALIDATION AND APPLICATION

For the experimental validation and application of the method, two different bainitic microstructures have been used; one corresponds to the recently developed nanobainite, a mixture of nano-scale plates of bainitic ferrite and films of retained austenite, obtained by isothermal transformation at 200°C, in a 0.7C-1.4Si-1.3Mn-1.0Cr-0.24Mo (wt.%) steel. Further details of the particularities of this new microstructure can be found elsewhere [3,4]. The other microstructure consists of a mixture of sub-micron laths of bainite and M/A (martensite/austenite) constituent obtained by continuous cooling after hot-rolling of a commercial 0.2C-1.0Si-1.6Mn-1.6Cr (wt.%) steel [31].

The experimental EBSD analyses for the identification of crystalline orientations were performed using a FEG-SEM JEOL JSM 6500F coupled to HKL CHANNEL 5 system (Oxford Instruments), operating at 20KV. Samples were ground and polished using 1 μm diamond paste and finished in colloidal silica suspension. Only ferrite with a lattice parameter of 2.866Å was indexed in the two microstructures, but it was possible to perform the parent reconstruction for the nanobainitic steel, obtaining the apparent PAGS as the average Feret diameter weighted to the grain area. The

experimental EBSD data were filtered to reduce the unnecessarily high resolution (number of data points used as input), so that the algorithm could run on a standard computer.

For the generation of simulated EBSD maps, codes have been implemented using the free and open-source MTEX toolbox [12] running in MATLAB [32]. The same tools have been used to code the algorithm that allows the calculation of the EGS from the simulated and the experimental EBSD maps; this is available on-line [33].

3-RESULTS AND DISCUSSION

3.1 EFFECT OF SIMULATION PARAMETERS

Fig. 4 shows the RSS vs. distance plot after applying the algorithm to simulated EBSD maps of Group 1. The corresponding analysis results are summarized in Table 4, from which it is clear, as expected, that the EGS (Effective Grain Size) increases as the austenite grain coarsens, when keeping step-size and number of grains to a constant value. The correction factor, i.e., the EGS relative to the apparent PAGS, holds a value of 80% approximately in these three cases. The effect of the other geometrical parameters in the EGS measurement is summarised from Fig. 5 to Fig. 7. In Fig. 5, simulated maps having the same apparent PAGS, 182 μm , and number of prior austenite grains, 9, but different step-sizes, are compared. It is clear that besides the increase of dispersion of data, the calculated EGS increases as, the step-size is decreased, i.e., the resolution improves.

The results on simulated maps having the same apparent PAGS, 182 μm , and step-size, 8 μm , but different number of prior austenite grains, are compared in Fig. 6. Three cases were selected, one with a small number of grains, 2, another with 9 and the third scenario with 30 grains, and the tendency observed is that the EGS decreases as the number of grains increases. However, when the number of grains and the resolution are high enough, the RSS vs. distance curves converge so that the EGS becomes constant at an intermediate value. This can be observed in Fig. 7, where, with a map of 30 prior austenite grains and a step-size of 8 μm , the EGS has already reached the value 148 μm (87% of the apparent PAGS), which does not change any more, regardless of the decrease of step-size or the

increase of number of grains. Therefore, if the measurement parameters for the EGS are appropriate, the apparent prior austenite grain size can be calculated as approximately 115% of the EGS.

It is clear that optimal results are obtained with a relatively large number of prior austenite grains, while the method is able to tolerate a relatively large step-size. In cases where EBSD maps contain a low number of prior austenite grains, this new method is still worthwhile to apply in a qualitative manner: the PAGS of different microstructures can be compared if the area scanned and the step-size have the same values in all tests. In such cases, the microstructures with higher PAGS will always yield a higher EGS because of both the higher PAGS per-se and the corresponding lower number of grains included in the area analyzed.

Table 1. Results on the EGS, Effective Grain Size, calculated from simulated EBSD maps according to Group 1 conditions in Table2.

Simulated map	Hexagon size (Apparent PAGS) [μm]	EGS [μm]	EGS relative to apparent PAGS
1	18	15	83%
2	91	71	78%
3	182	144	79%

3.2 EXPERIMENTAL VALIDATION OF THE METHOD

The simulated EBSD maps are a simplification of a bainitic microstructure in which different morphologic/crystallographic factors affecting a real microstructure have been omitted: subunits of bainitic ferrite are lath or plate shaped, subunits of variants with low misorientation are associated forming blocks, and blocks sharing the habit plane occur together forming packets; austenite grains may have been twinned; the orientation relationship between variants present spread values; and there might even be a strong variant selection [3,14,31,34,35,36]. Therefore, the method needs to be experimentally validated in bainitic/martensitic microstructures with a known PAGS to verify its applicability despite the above-mentioned factors. In this case, a nanobainitic steel has been chosen. The PAGS has been calculated first through the manual parent reconstruction of the experimental

EBSD map, by means of the assessment of the pole figures from selected areas of the orientation map, e.g. Fig. 8. The reconstructed map, Fig. 9, presents a total of 8 austenite grains, the apparent PAGS (calculated including edge grains) being equal to 33 μm .

Fig. 10 (a) shows the DDF plot obtained after applying the method just described to the EBSD map after filtering to reduce the resolution and hence the computation time. As in the case of the DDF of simulated EBSD maps, the misorientation distribution evolves from spike-like at low distances to a Mackenzie-Handscomb distribution at larger distances. However, it is evident that peaks at low distances have a different frequency density than in the simulated EBSD map in Fig. 2, especially near 0° , whose peak is caused by data points belonging to the same bainitic ferrite subunit. The EGS in this case is about 31 μm , as can be observed in the curve of Fig. 10 (b), which is a value higher than 90% of the apparent PAGS, a result consistent with the fact that only a few grains have been used for the measurement of the EGS, as already discussed.

Moreover, in order to check further the reliability of the method, a modified algorithm has been implemented, consisting in the calculation of the apparent PAGS of only one of the revealed PAG, Φ , in Fig. 9, which has a Feret diameter of 22.6 μm . The modified algorithm collected the distances and misorientations between data points inside the PAG and data points of the whole map, but not between data points outside the PAG. The calculated EGS, is about 20 μm , a value also higher than 90% of the Feret diameter, see Fig. 10 (c).

3.3 APPLICATION OF THE METHOD

The method has been applied to a commercial hot-rolled air-cooled bainitic steel with a microstructure formed from a mixture of sub-micron laths of bainitic ferrite and a M/A constituent. The unreliable indexation of retained austenite as well as the difficulty of performing an unambiguous parent reconstruction due to the strong variant selection, with the absence of some variants and a large spread of orientation inside each PAG (see Fig. 11 as an example of Pole Figure) make this new

method a unique and easy opportunity to obtain the PAGS from EBSD data, under such unfavorable circumstances. On the other hand, the hot-rolling temperature, of this heat-treated steel, above A_3 , ensures a complete recrystallization of the austenite grains before bainitic transformation, i.e. austenite grains are randomly oriented, which is a condition for the viability of the procedure.

The low magnification of the EBSD map in Fig. 12 (a) makes it more representative of the whole microstructure (i.e. including a large number of prior austenite grains). It is worth mentioning that although the EBSD map was recorded with a step size of $1\ \mu\text{m}$, it was also possible and necessary to apply a filter to the EBSD dataset to reduce the number of data points before the computation of the algorithm, Fig. 12 (b), increasing the step-size up to $2.8\ \mu\text{m}$. Increasing the step-size makes the method more valuable, since it is common practice to work at low resolution to keep a balance between scanned area and test duration. To check whether the solution has converged so that the apparent PAGS can be calculated as the 115% of the EGS, the EBSD data was again modified in the post-process in two different ways: keeping the same area analyzed while changing the step size, and keeping the step size while reducing the area, see Fig. 12 (c). The results thus obtained proved that the three curves overlap and result in a EGS equal to $42\ \mu\text{m}$, so that the apparent PAGS of the hot-rolled air-cooled bainitic steel must be close to $115\% \cdot 42\ \mu\text{m} = 48.30\ \mu\text{m}$.

4-CONCLUSIONS

An algorithm for the post-processing of EBSD data has been assessed as a method to calculate automatically the prior austenite grain size in bainitic/martensitic microstructures. It has been applied to simulated EBSD maps and also to experimental EBSD maps obtained from a nanobainitic steel and from a sub-micron bainitic microstructure obtained in a commercial hot-rolled air-cooled steel. The method has been proven to be robust and insensitive to the step-size and the number of prior austenite grain sizes when a large enough area is analyzed that the solution is convergent, and information on the necessary step size and number of grains in a uniform hexagonal grain structure has been obtained. In this case, the apparent Prior Austenite Grain Size can be calculated as 115% of the EGS.

The obtained results are promising, the main advantage of the proposed method being its suitability for analysis of time-optimized low magnification EBSD scans, where a huge area is analyzed, resulting in an accurate value of the PAGS representative of the whole microstructure. Moreover, the method can yield qualitative results suitable to compare the prior austenite grain size of different microstructures, in cases where the area analyzed is not high enough for an accurate measurement.

Although the new method has been experimentally validated on two different microstructures containing bainite, the crystallographic similarities between bainite and martensite would allow its applicability to fully martensitic microstructures.

The tool developed to perform the analysis is available to be downloaded for free.

5-ACKNOWLEDGEMENT

The authors gratefully acknowledge the support of the Spanish Ministry of Economy and Competitiveness for funding this research under the contract IPT-2012-0320-420000. L.M.-R. also acknowledges the Spanish Ministry of Economy and Competitiveness for financial support in the form of a PhD research grant (FPI-Ref. BES-2011-044186).

TABLE OF ACRONYMS

DDS: Distance-Disorientation Function

EBSD: Electron Backscatter Diffraction

EGS: Effective Grain Size

KS-OR: Kurdjumov-Sachs Orientation Relationship

OR Orientation Relationship

PAG: Prior Austenite Grain

PAGB: Prior Austenite Grain Boundary

PAGS: Prior Austenite Grain Size

RSS: Residual Sum of Squares

FIGURE CAPTIONS

Fig.1 Example of Distance-Disorientation Function (DDF) plot from a simulated EBSD map containing 30 hexagons of 91 μm size, as an example.

Fig. 2 Mackenzie-Handscomb distribution and misorientation distributions at different distances from a simulated EBSD map containing 30 hexagons of 91 μm size, as an example.

Fig. 3 Drawing showing simulated Prior Austenite Grain (PAG) containing bainitic ferrite (BF) variants. Only 6 enlarged EBSD data points are shown for the sake of clarity. d1 and d3 are distances separating data points (indexed as ferrite) with one of the K-S inter-variant misorientations listed in Table 1, as they belong to the same PAG; whereas d2 and d3 are distances between data points (indexed as ferrite) randomly misoriented, as they belong to different PAG

Fig. 4 Residual Sum of Squares (RSS) vs. distance of three simulated EBSD maps containing 30 grains and with a step-size of 4 μm , for three different Prior Austenite Grain Size (PAGS). Red lines indicate the measured Effective Grain Size Value (EGS).

Fig. 5 Residual Sum of Squares (RSS) vs. distance of three simulated EBSD maps containing 9 grains and with an apparent Prior Austenite Grain Size (PAGS) of 182 μm , for three different step-size. Red lines indicate the measured Effective Grain Size Value (EGS).

Fig. 6 Residual Sum of Squares (RSS) vs. distance of three simulated EBSD maps with a step-size of 8 μm and an apparent Prior Austenite Grain Size (PAGS) of 182 μm , for three different number of grains. Red lines indicate the measured Effective Grain Size Value (EGS).

Fig. 7 Residual Sum of Squares (RSS) vs. distance of three simulated EBSD maps with an apparent Prior Austenite Grain Size (PAGS) of 182 μm and different number of grains and step-size. Red line indicates the measured Effective Grain Size Value (EGS).

Fig. 8 Pole figure from a selected area of the orientation map from the nanobainitic steel. The selected area corresponds to one only Prior Austenite Grain (PAG)

Fig. 9 Prior Austenite Grain Boundaries (PAGB), black lines, of the nanobainitic steel reconstructed parent microstructure, on its EBSD orientation map. Φ symbol indicates the grain used for the modified algorithm, explained in the main text

Fig. 10 Based on the nanobainitic steel EBSD map from Fig. 9. (a) Distance-Disorientation Function (DDF); (b) Residual Sum of Squares (RSS) vs. distance; (c) RSS vs. distance, after applying a modified algorithm to calculate the Effective Grain Size (EGS) of just one grain, Φ in Figure 9, with an apparent Prior Austenite Grain Size (PAGS) of 22.6 μm . Red lines indicate the measured Effective Grain Size Value (EGS).

Fig. 11 Pole figure from a selected area of the orientation map from the sub-micron bainite. The featured planes belong to bainitic ferrite laths from the same Prior Austenite Grain (PAG); it is noticeable the absence of some variants

Fig. 12 (a) EBSD orientation map of the hot-rolled air-cooled steel and (b) the same map after the application of a filter to reduce the resolution (number of data points); (c) Residual Sum of Squares (RSS) between vs. distance of the map in Fig. 12 (a) after three different modifications during the data post-processing. Red line indicates the measured Effective Grain Size Value (EGS).

REFERENCES

- 1 Gladman T (1997) The physical metallurgy of microalloyed steels. Institute of Materials, London
- 2 Matsuzaki A, Bhadeshia HKDH (1999) Effect of austenite grain size and bainite morphology on overall kinetics of bainite transformation in steels. *Mater Sci Technol* 15:518–522
- 3 Garcia-Mateo C, Caballero FG, Bhadeshia HKDH (2003) Acceleration of low-temperature bainite. *ISIJ Int* 43:1821–1825
- 4 Garcia-Mateo C, Sourmail T, Caballero FG, et al. (2014) Nanostructured steel industrialisation: plausible reality. *Mater Sci Technol* 30:1071-1078
- 5 Vander Voort GF (1984) *Metallography: principles and practice*. McGraw-Hill Book, New York
- 6 García De Andrés C, Bartolomé MJ, Capdevila C, San Martín D, Caballero FG, López V (2001) Metallographic techniques for the determination of the austenite grain size in medium-carbon microalloyed steels. *Mater Charact* 46:389–398
- 7 Lozinskii MG (1961) *High temperature metallography*. Pergamon, Oxford, p 241
- 8 Okamoto M, Miyagawa O, Saga T (1966) High temperature microscope observation of the austenite grain size of steels. *Trans Jpn Inst Met* 7:217–223
- 9 Modin H, Modin S (1973) *Metallurgical microscopy*. Butterworths, London, pp 181-183
- 10 Gourgues-Lorenzon, A.F. Application of electron backscatter diffraction to the study of phase transformations. *Int. Mater. Rev.* **2007**, 52 (2), 65-128.
- 11 Patala, S.; Mason, J.K.; Schuh, C.A. Improved representations of misorientation information for grain boundary science and engineering. *Prog. Mater. Sci.* **2012**, 57 (8), 1383-1425.

-
- 12 Bachmann F, Hielscher R, Schaeben H (2010) Texture analysis with MTEX - free and open source software toolbox. *Solid State Phenom* 160:63-68
- 13 Kurdjumow G, Sachs G (1930) Über der Mechanismus der Stahlhärtung (On the mechanism of hardening of steel). *Z Physik* 64:325-343
- 14 Furuhashi T, Kawata H, Morito S, Maki T (2006) Crystallography of upper bainite in Fe–Ni–C alloys. *Mater Sci Eng A* 431:228-236
- 15 Nishiyama Z (1934) X-ray investigation of the mechanism of the transformation from face-centred cubic lattice to body-centred cubic. *Sci Rep Tohoku Imperial Univ* 23:637-664
- 16 Wassermann G (1935) Über den Mechanismus der $\alpha \rightarrow \gamma$ Umwandlung des Eisens (On the mechanism of the $\alpha \rightarrow \gamma$ transformation of iron). *Mitteilungen aus dem Kaiser Wilhelm Institut für Eisenforschung* 17:149-155
- 17 Germain L, Gey N, Mercier R, Blaineau P, Humbert M (2012) An advanced approach to reconstructing parent orientation maps in the case of approximate orientation relations: Application to steels. *Acta Mater* 60:4551-4562
- 18 Yardley VA, Payton EJ (2014) Austenite–martensite/bainite orientation relationship: characterisation parameters and their application. *Mater Sci Technol* 30:1125-1130
- 19 HKL CHANNEL 5 software, version 5.0.9.0, 1998-2006 HKL Technology A/S (Oxford Instruments plc, Tubney Woods, Abingdon, Oxon OX13 5QX, UK)
- 20 Cayron C, Artaud B, Briottet L (2006) Reconstruction of parent grains from EBSD data. *Mater Charact* 57:386-401
- 21 Tari V, Rollett AD, Beladi H (2013) Back calculation of parent austenite orientation using a clustering approach. *J Appl Crystallogr* 46:210-215

-
- 22 Abbasi M, Nelson TW, Sorensen CD, Wei L (2012) An approach to prior austenite reconstruction. *Mater Charact* 66:1-8
- 23 Miyamoto G, Iwata N, Takayama N, Furuhashi T (2010) Mapping the parent austenite orientation reconstructed from the orientation of martensite by EBSD and its application to ausformed martensite. *Acta Mater* 58:6393-6403
- 24 Bernier N, Bracke L, Malet L, Godet S (2014) An alternative to the crystallographic reconstruction of austenite in steels. *Mater Charact* 89:23-32
- 25 Payton EJ, Aghajani A, Otto F, Eggeler G, Yardley VA (2012) On the nature of internal interfaces in a tempered martensite ferritic steel and their evolution during long-term creep. *Scr Mater* 66:1045-1048. doi:10.1016/j.scriptamat.2012.02.042
- 26 Jafarian HR, Borhani E, Shibata A, Terada D, Tsuji N (2011) Martensite/austenite interfaces in ultrafine grained Fe-Ni-C alloy. *J Mater Sci* 46:4216-4220
- 27 Brahme A, Staraselski Y, Inal K, Mishra RK (2012) Determination of the minimum scan size to obtain representative textures by electron backscatter diffraction. *Metall Mater Trans A* 43:5298-5307
- 28 Beausir, B.; Fressengeas, C.; Gurao, N.P.; Toth, L.S.; Suwas, S. Spatial correlation in grain misorientation distribution. *Acta Mater.* **2009**, 57 (18), 5382-5395
- 29 Mackenzie JK (1958) 2nd paper on statistics associated with the random misorientation of cubes. *Biometrika* 45:229-240
- 30 Handscomb DC (1958) On the random misorientation of two cubes, *Canad J Math* 10:85-88
- 31 Caballero FG, Roelofs H, Hasler S, et al. (2012) Influence of bainite morphology on impact toughness of continuously cooled cementite free bainitic steels. *Mater Sci Technol* 28:95-102
- 32 MATLAB (MathWorks, Inc., Natick, MA, USA)

33 Morales-Rivas L (2013) EBSD Distance-Disorientation Distribution 3D plot, MATLAB Central File Exchange. Retrieved July 15, 2014

<http://www.mathworks.com/matlabcentral/fileexchange/40789-ebsd-distance-disorientation-distribution-3d-plot>

34 Bramfitt S (1990) A perspective on the Morphology of Bainite. Metall Trans A 21 A:817-829

35 Krauss G, Thompson SW (1995) Ferritic microstructures in continuously cooled low-carbon and ultralow-carbon steels. ISIJ Int 35:937-945

36 Zajac S, Komenda J, Morris P, Dierickx P, Matera S and Penalba Diaz S (2005) Quantitative structure–property relationship for complex bainitic microstructures. Technical Steel Research, European Commission, contract No 7210-PR/247, Final report. ISBN: 92-894-9206-6.

<http://bookshop.europa.eu/en/quantitative-structure-property-relationships-for-complex-bainitic-microstructures-pbKINA21245/>

Figure 1

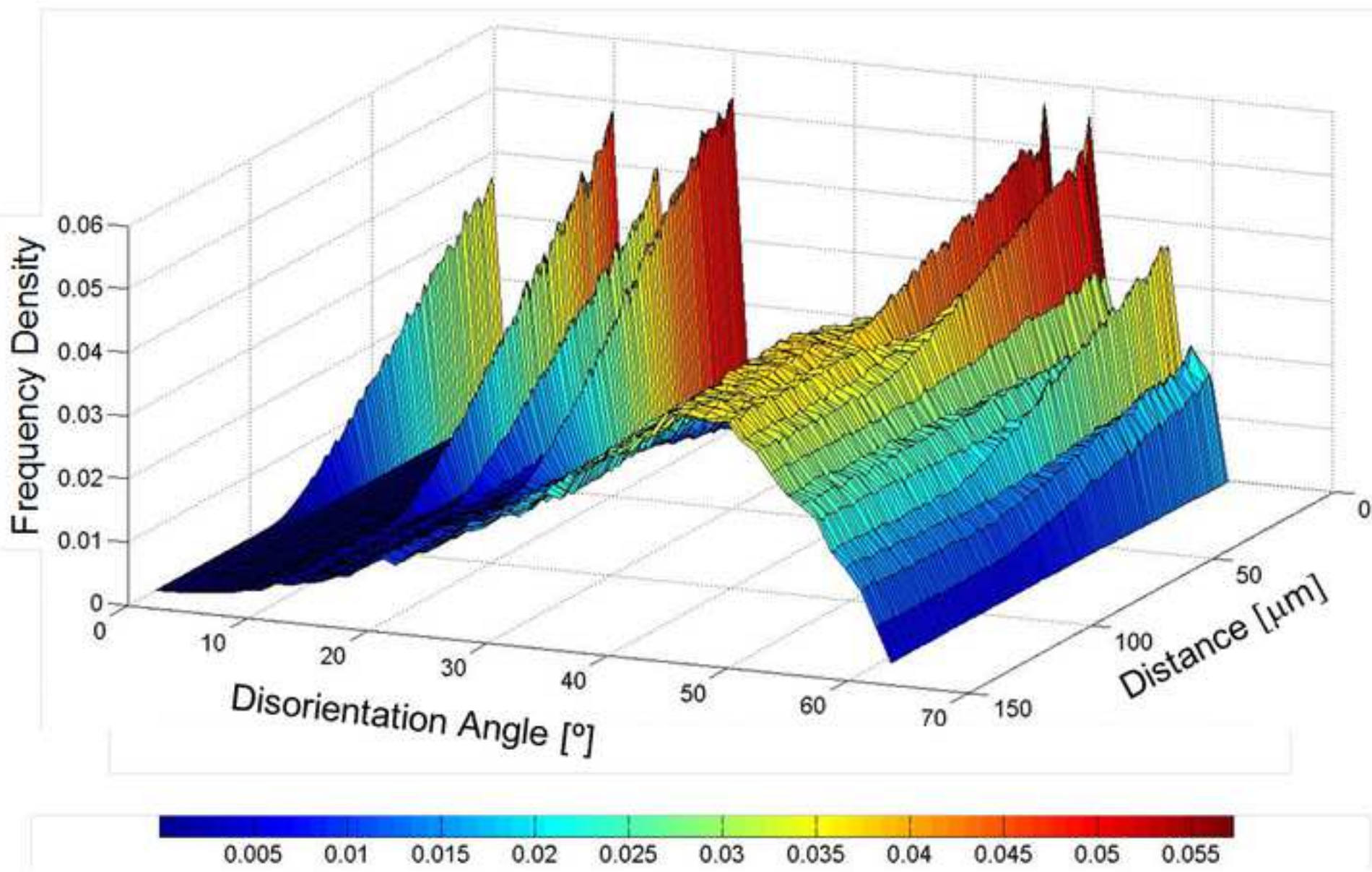






Figure 2

-  Mackenzie-Handscomb distribution
-  Distribution of misorientations at maximum distance
-  Distribution of misorientations at intermediate distances
-  Correlated misorientation distribution

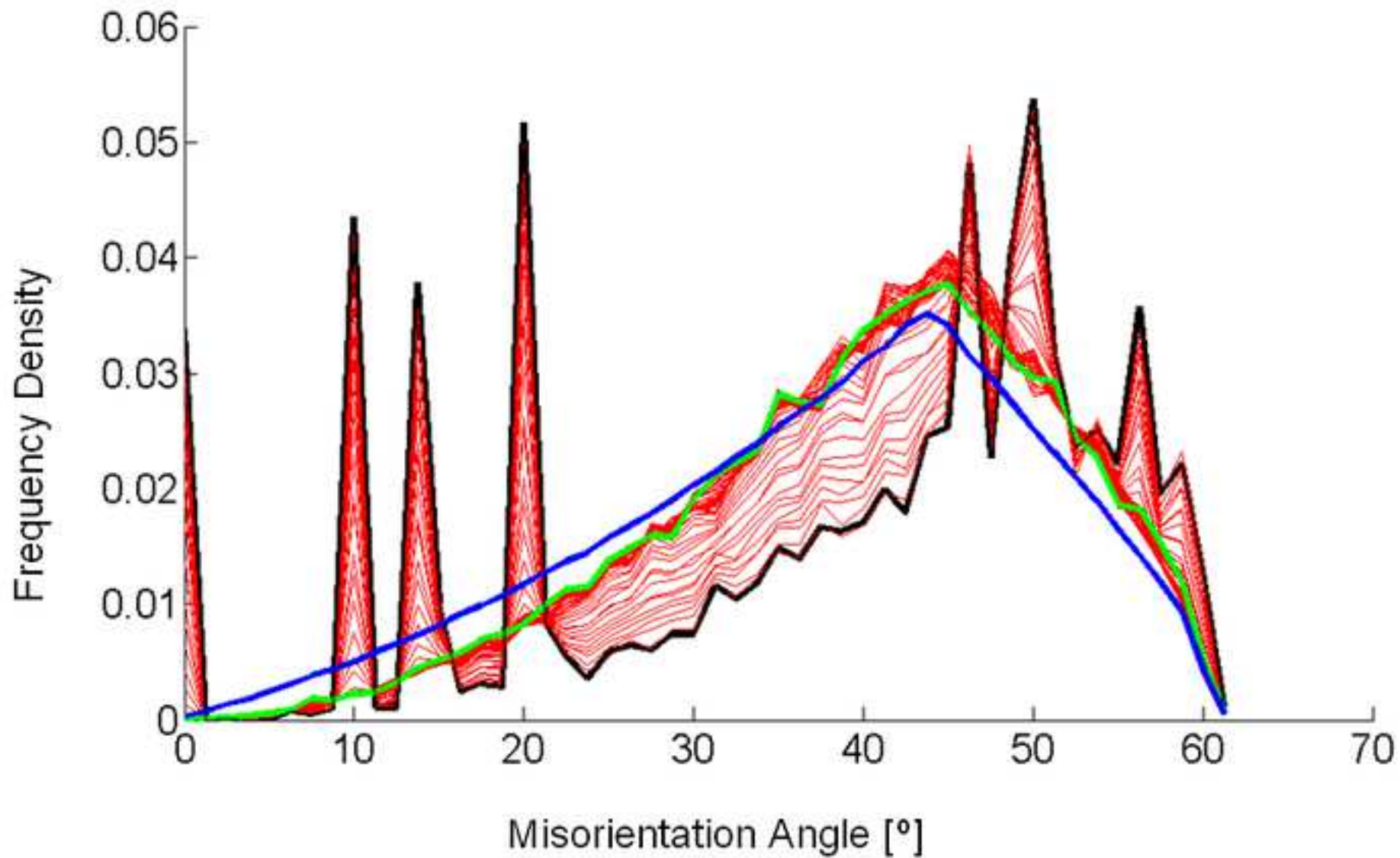


Figure 3

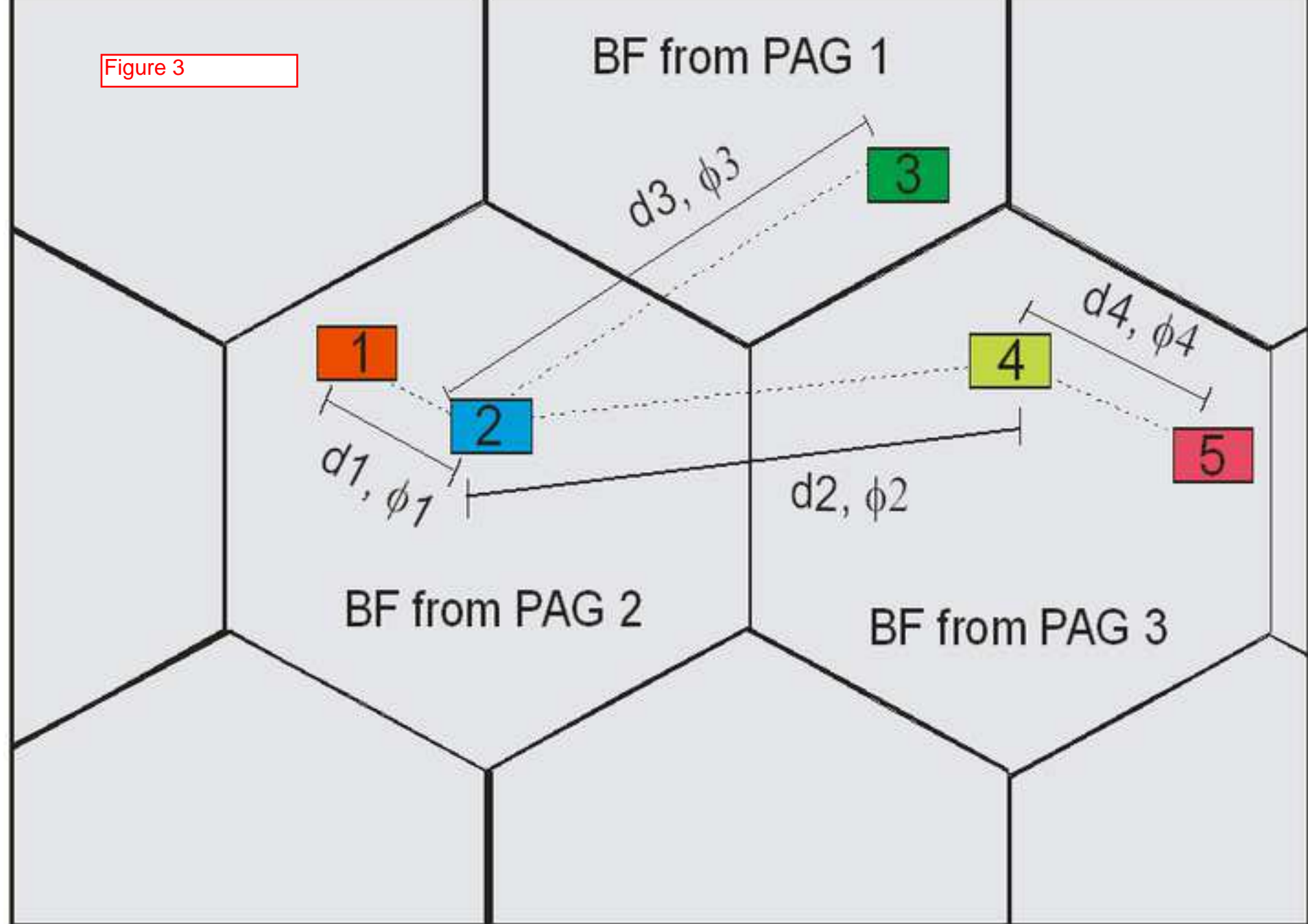


Figure 4

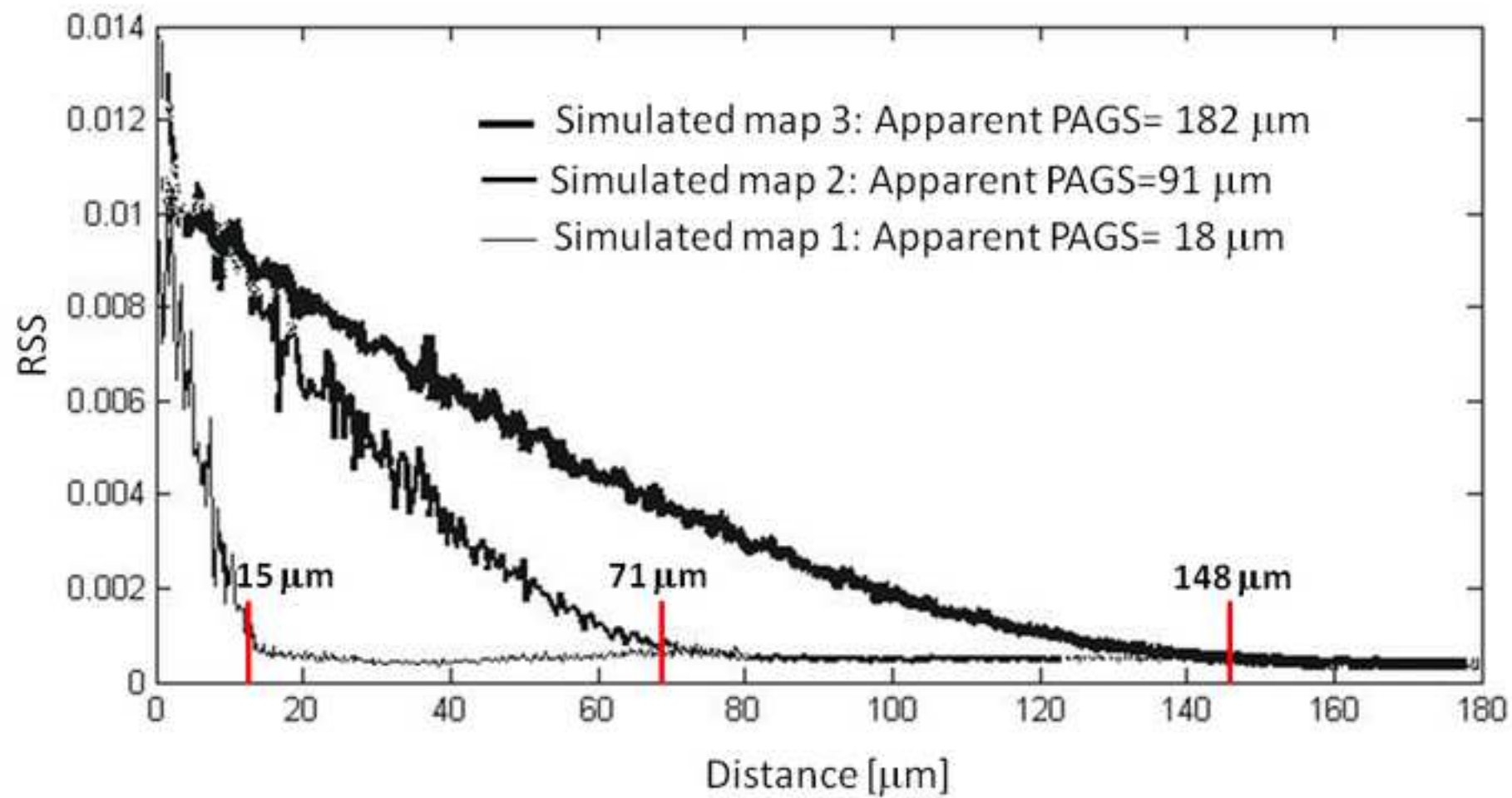


Figure 5

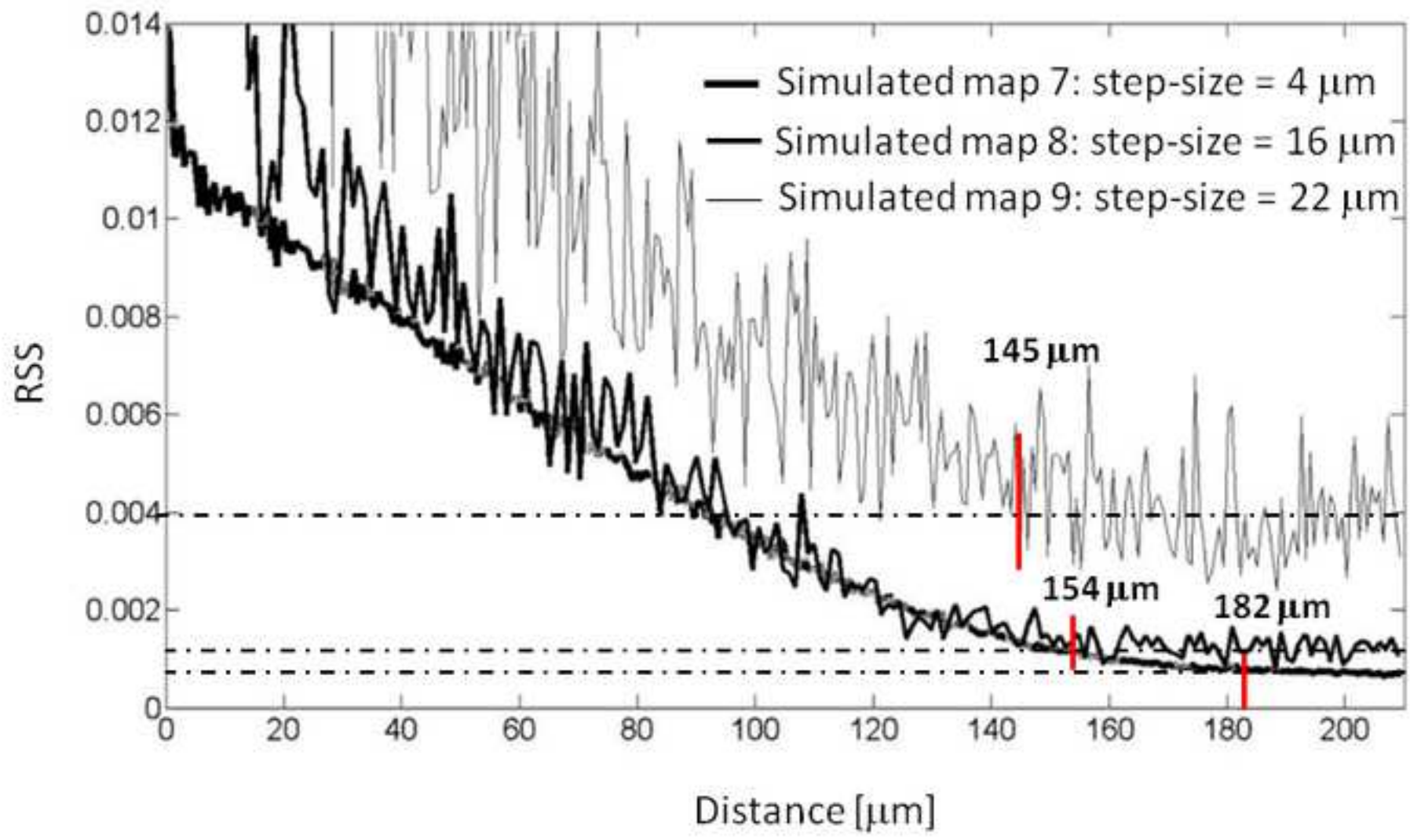


Figure 6

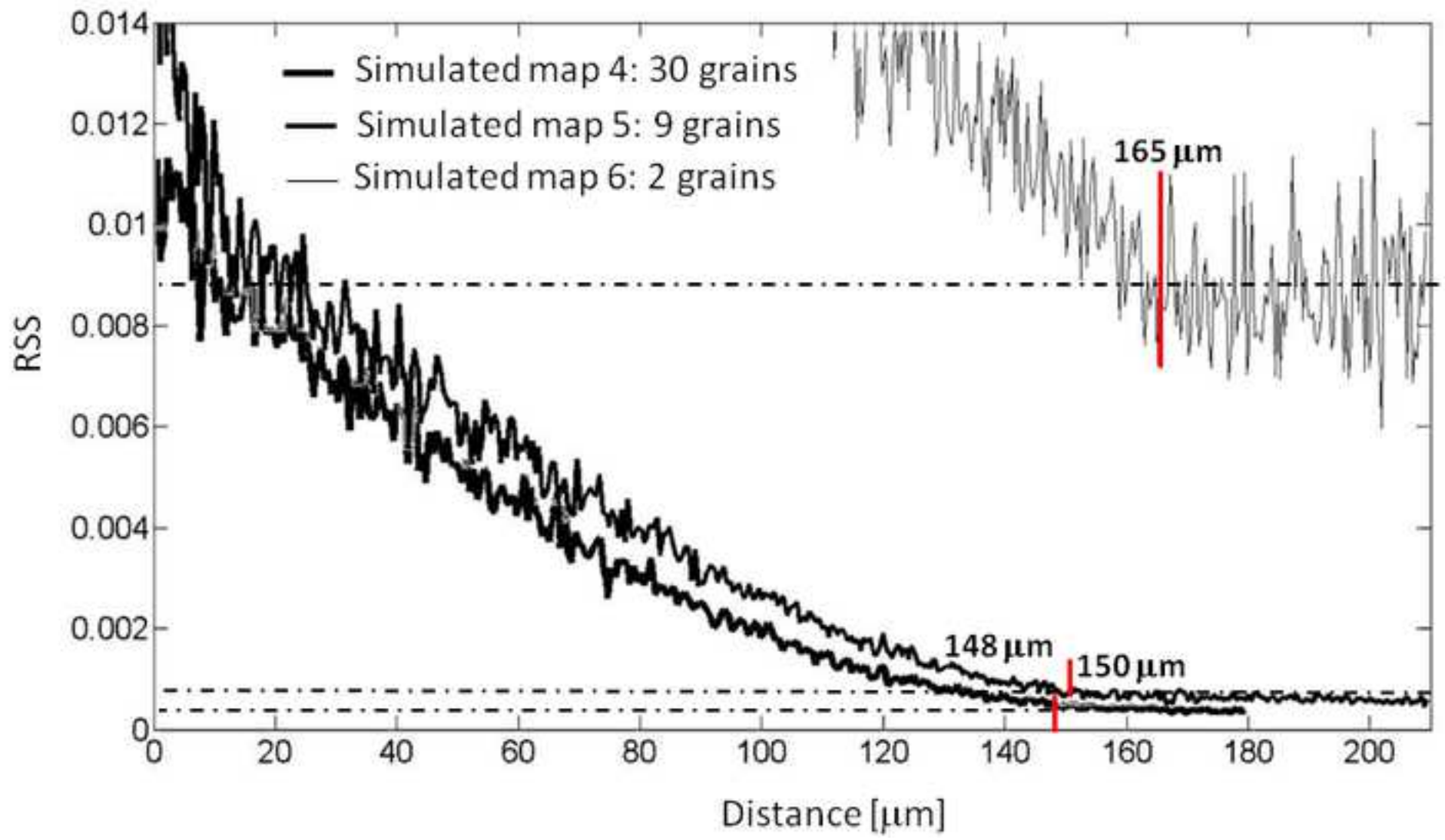


Figure 7

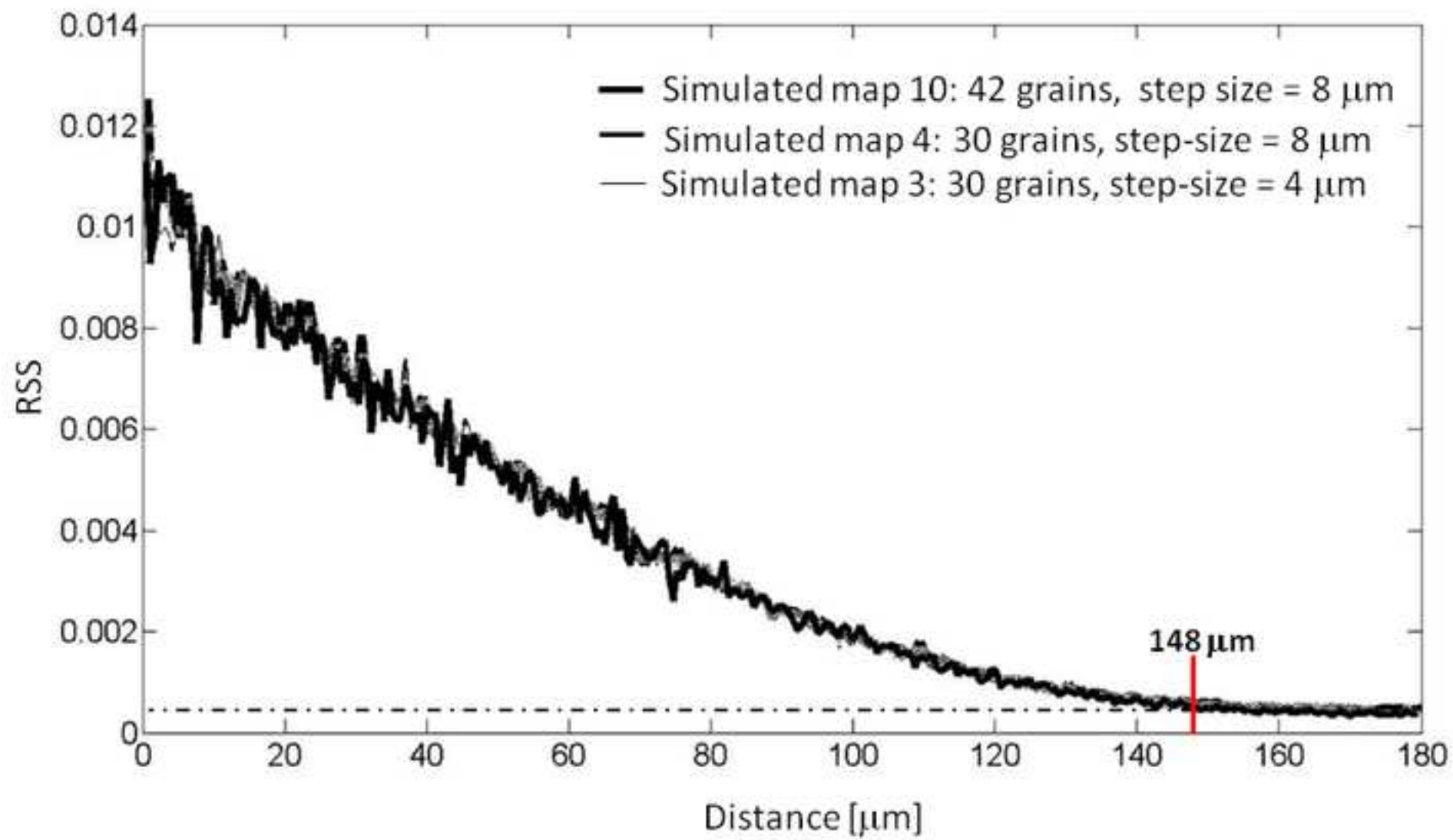


Figure 8

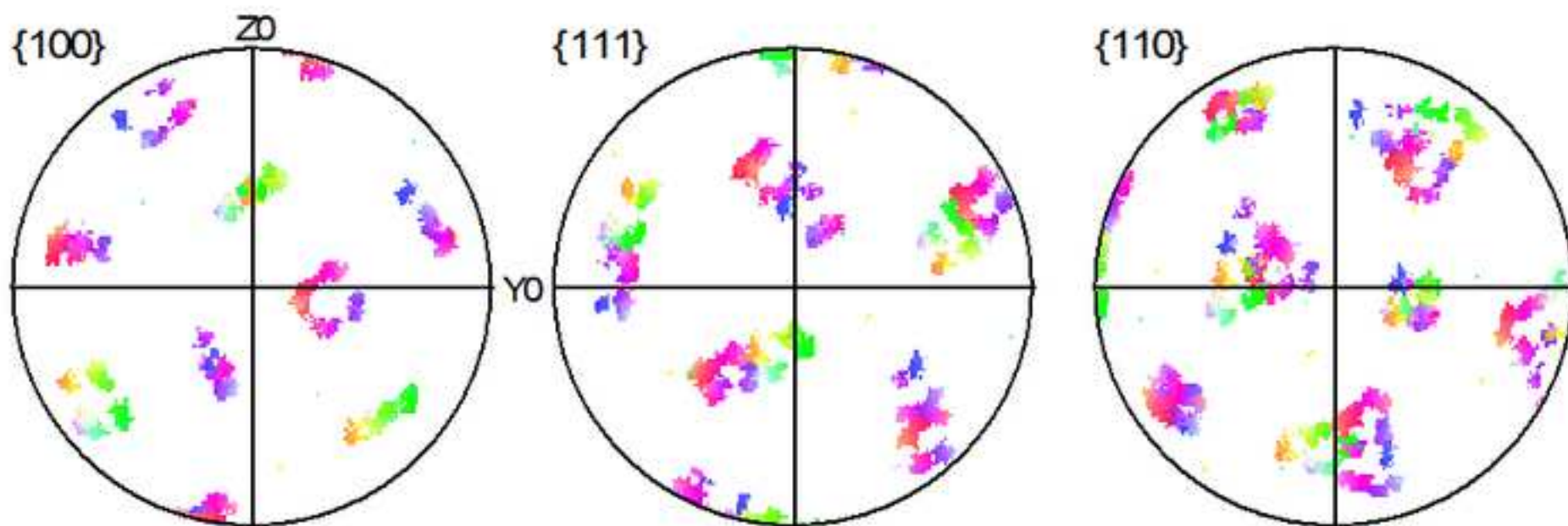
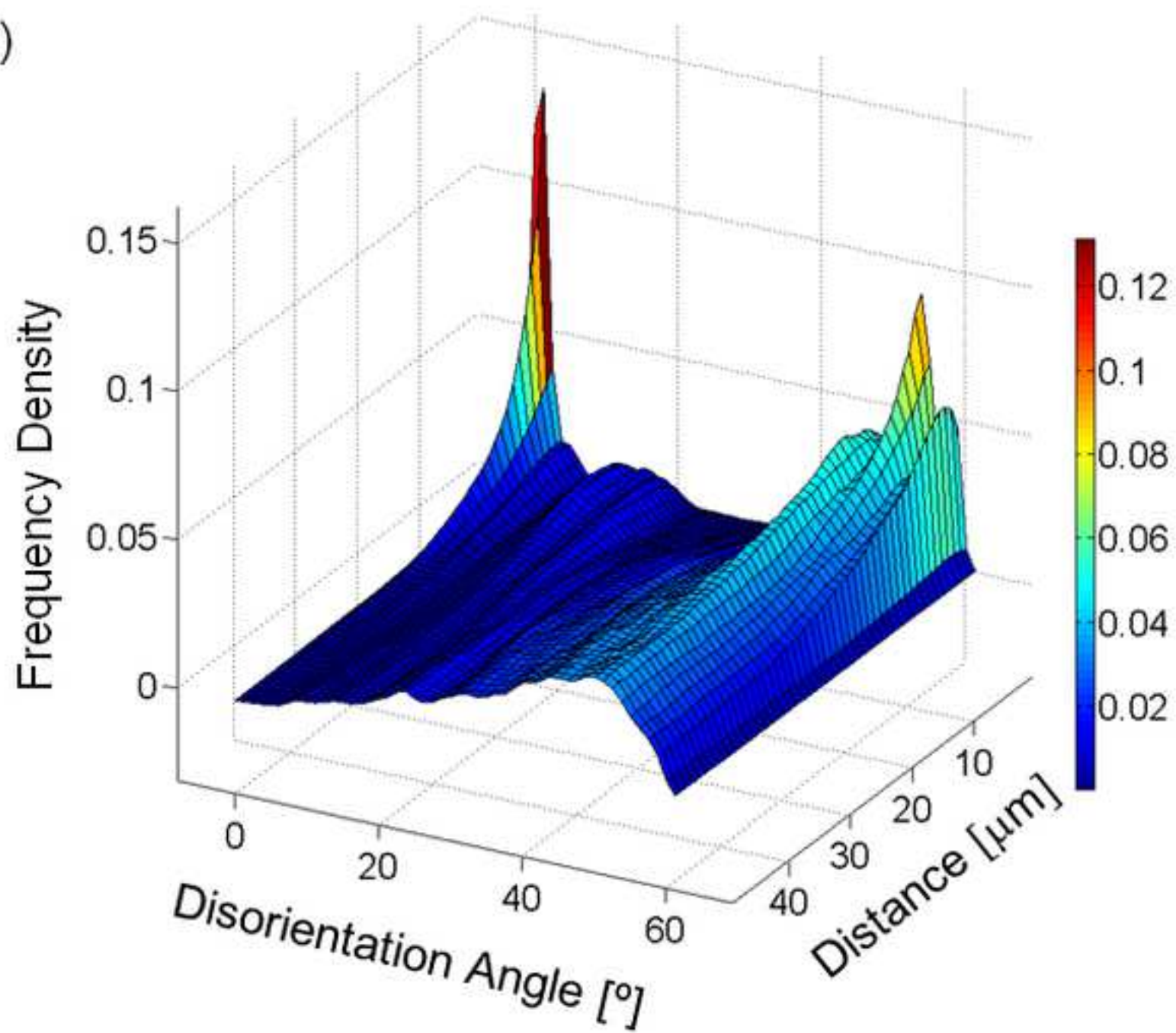


Figure 9



(a)



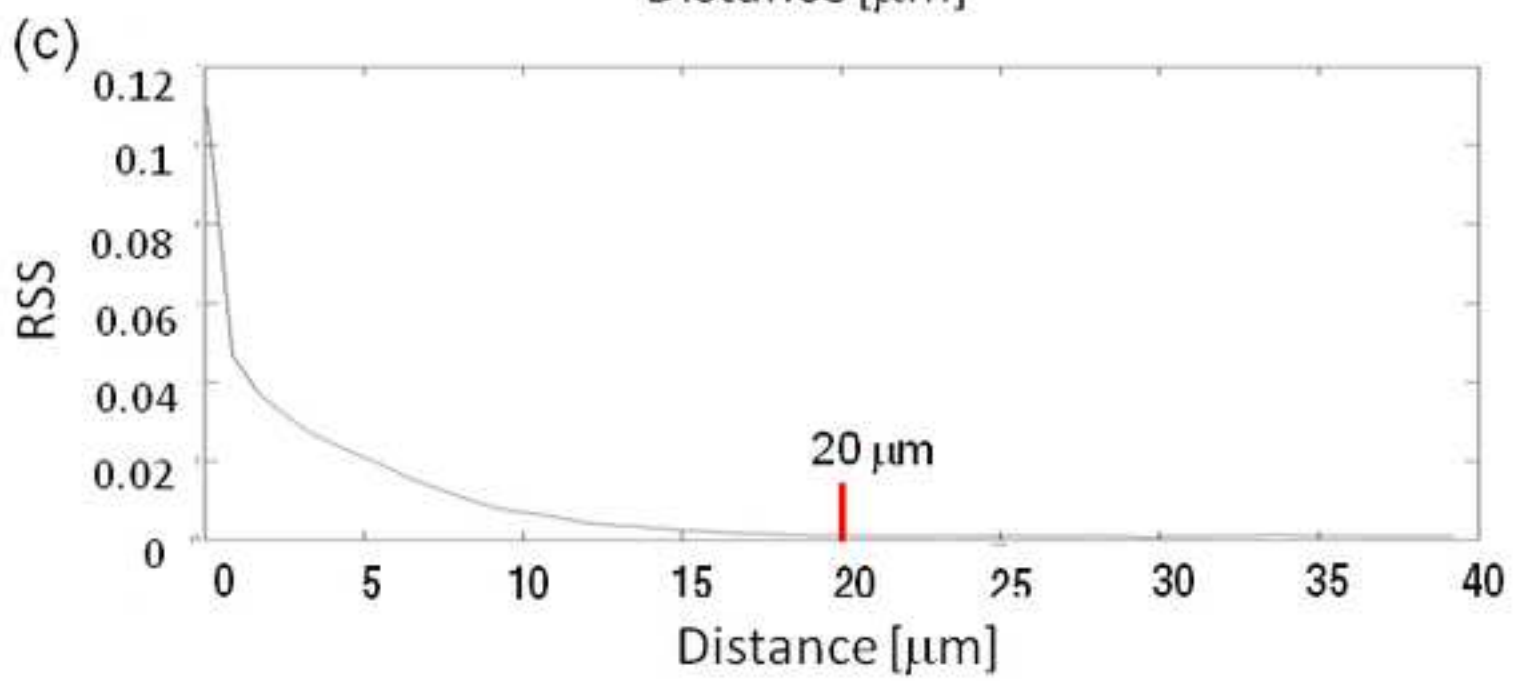
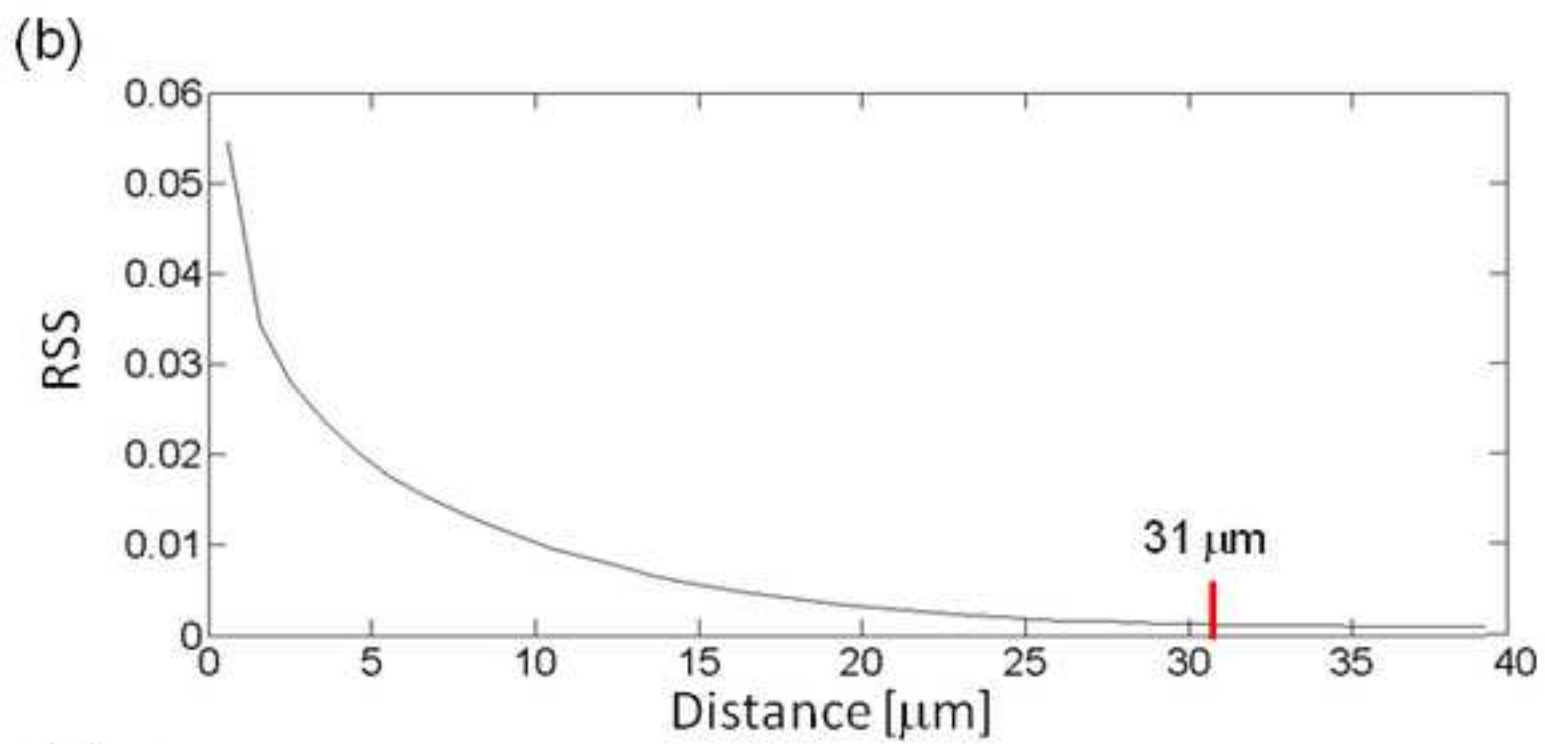


Figure 11

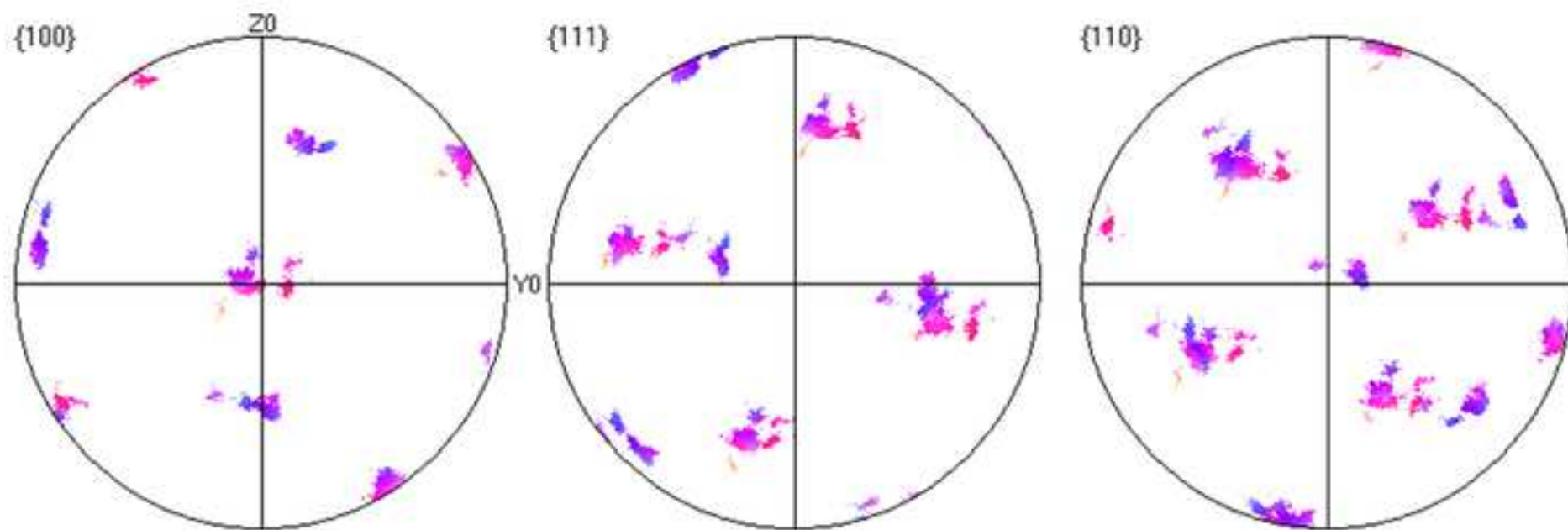


Figure 12 a

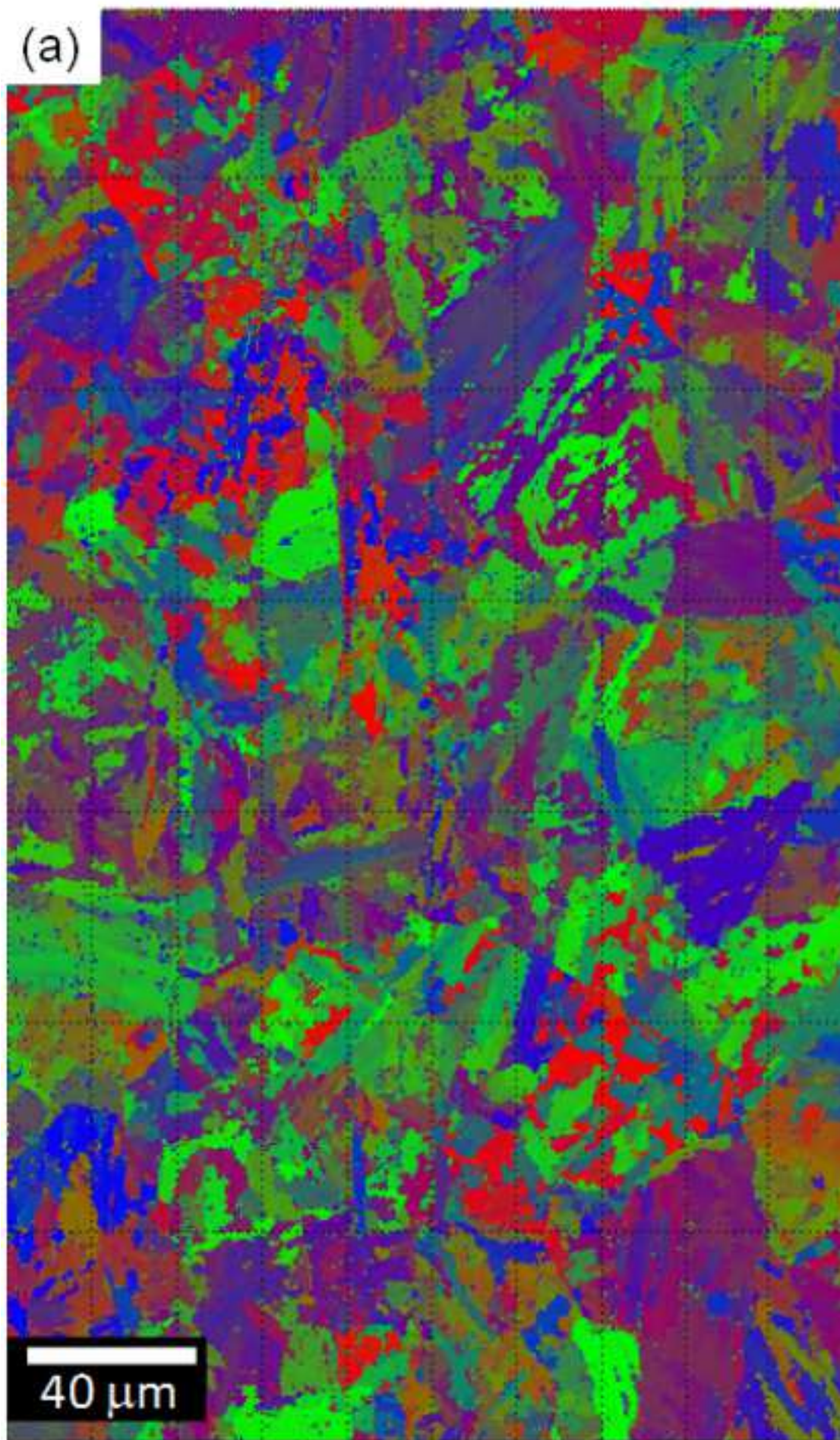
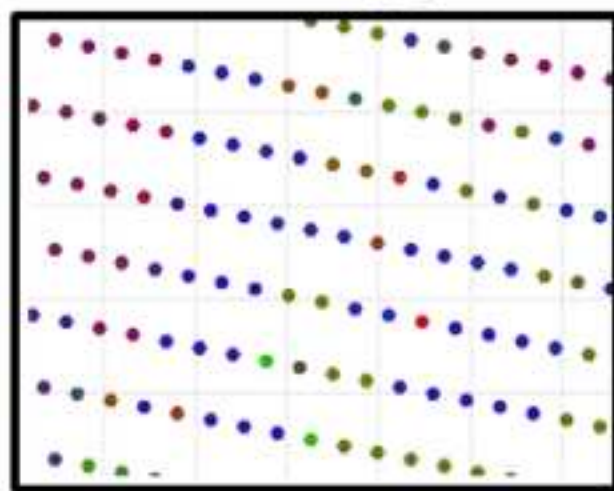
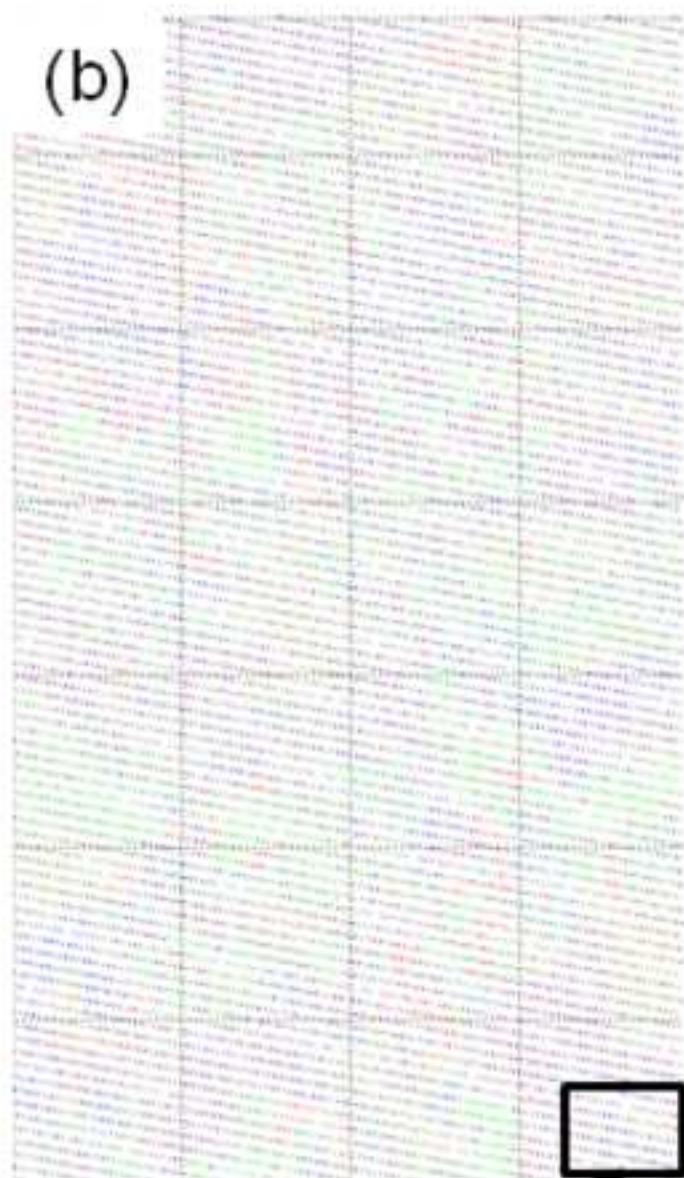


Figure 12 b



10 μm

Figure 12 c

